

# A Temporally Explicit Production Efficiency Model for Fuel Load Allocation in Southern Africa

Christelle Hély,<sup>1,2,\*</sup> Kelly K. Caylor,<sup>1,3</sup> Peter Dowty,<sup>1</sup> Samuel Alleaume,<sup>1,4</sup> Robert J. Swap,<sup>1</sup> Hank H. Shugart,<sup>1</sup> and Christopher O. Justice<sup>5</sup>

<sup>1</sup>Environmental Sciences Department, University of Virginia, 291 McCormick Road, Charlottesville, Virginia 22904-4123, USA; <sup>2</sup>CEREGE, CNRS, Université Aix-Marseille Paul Cézanne, B.P. 8013545, Aix-en-Provence cedex 4, France; <sup>3</sup>Department of Civil and Environmental Engineering, Princeton University, Princeton, New Jersey 08544, USA; <sup>4</sup>CEMAGREF, 3275 route de Cézanne, CS40061, Aix-en-Provence, 13182, France; <sup>5</sup>Geography Department, University of Maryland, College Park, Maryland 20742, USA

## ABSTRACT

We present a regional fuel load model (1 km<sup>2</sup> spatial resolution) applied in the southern African savanna region. The model is based on a patch-scale production efficiency model (PEM) scaled up to the regional level using empirical relationships between patch-scale behavior and multi-source remote sensing data (spatio-temporal variability of vegetation and climatic variables). The model requires the spatial distribution of woody vegetation cover, which is used to determine separate respiration rates for tree and grass. Net primary production, grass and tree leaf death, and herbivory are also taken into account in this mechanistic modeling approach. The fuel load model has been calibrated and validated from independent measurements taken from savanna vegetation in Africa southward from the equator. A sensitivity analysis on the effect of climate variables (incoming radiation, air temperature, and precipitation) has been conducted to demonstrate the strong role that

water availability has in determining productivity and subsequent fuel load over the southern African region. The model performance has been tested in four different areas representative of a regional increasing rainfall gradient—Etosha National Park, Namibia, Mongu and Kasama, Zambia, as well as in Kruger National Park, South Africa. Within each area, we analyze model output from three different magnitudes of canopy coverage (<5, 30, and 50%). We find that fuel load ranges predicted by the model are globally in agreement with field measurements for the same year. High rainfall sustains green herbaceous production late in the dry season and delays tree leaf litter production. Effect of water on production varies across the rainfall gradient with delayed start of green material production in more arid regions.

**Key words:** vegetation modeling; savannas; primary production; NDVI; climate; tree cover; fire.

## INTRODUCTION

Savanna ecosystems cover approximately 20% of the Earth's land surface, and 40% of Africa (Atjay and others 1987). Annually, about 2.5 GT of dry

matter are consumed in tropical savanna fires (Delmas and others 1991; Dwyer and others 2000). African savannas cover 1,184 Mha, or 48% of global savannas, and represent a region with the largest area of recent fires, burning an average of 311 Mha y<sup>-1</sup> in the 1980s (Mouillot and Field 2005). Emissions from southern African savanna fires, both natural and man-made, provide an

Received 16 November 2005; accepted 10 July 2007; published online 1 September 2007.

\*Corresponding author; e-mail: hely@cerege.fr

important contribution to the atmospheric chemistry of the region (Scholes and Andreae 2000). The sensitivity of southern African savannas to regional climate change and the consequences of current and future land-use change has been the focus of a number of recent international research activities (Desanker and others 1997; Scholes and others 2002; Swap 2002).

Previous studies on vegetation fires and carbon emissions have identified available fuel load to be one of the most variable factors in terms of spatial and temporal distributions (Lindesay and others 1996). This is likely due to the mixed life form, spatially heterogeneous vegetation found in southern African savannas (Scholes and Walker 1993). Because available fuel load is the balance between spatially and temporally explicit processes such as net primary production (NPP) litterfall, litter decay and herbivory, a mechanistic modeling approach for fuel load estimation is necessary.

Several ecosystem process models estimate terrestrial net primary production and carbon fluxes. In a comparative analysis, Cramer and others (1999) identify three major groups of models. The first group uses satellite data to determine the temporal behavior of the photosynthetically active tissue necessary for NPP estimates. In these models, the time of interest is limited to that of the satellite archive (for example, the Carnegie Ames Stanford Approach (CASA) by Potter and others (1993) and the GLOBAL production efficiency model (GLOPEM) by Prince and Goward (1995)). The second group of models simulates the biogeochemical fluxes on the basis of soil and climate characteristics, using either vegetation maps or biogeography models to prescribe vegetation structure (for example, the BIOME- BioGeoChemical cycles model (BIOME-BGC) by Hunt and others (1996) and CARAIB (Warnant and others 1994)). Such models can only describe functional changes within particular vegetation types and thereby ignore the possible effects of vegetation redistribution and their associated NPP changes. The third group of terrestrial net primary productivity models simulates changes in both ecosystem structure (vegetation distribution and phenology) and function (biogeochemistry). Generally, equilibrium between climate and vegetation is assumed (for example, BIOME3 (Haxeltine and Prentice 1996), DOLY (Woodward and others 1995)), but the models can also be turned into dynamical global vegetation models (DGVM). Except in some recent attempts of taking into account human activities (Brovkin and others 2004), these models deal with potential vegetation.

In the perspective of using an existing model for fuel load estimates in tropical savannas ecosystems, all these models share three main weak points: (1) They present a coarse spatial resolution ( $1^\circ \times 1^\circ$  for most of them, except GLOPEM ( $8 \times 8$  km resolution, Prince and Goward 1995)), which cannot reduce the overall uncertainties in savanna fire emissions. (2) In these models the vegetation is either real vegetation but mainly fixed and prescribed through vegetation classes (biomes, ecotypes, or classes using percentages of  $C_3$  versus  $C_4$  plants), or dynamic but in that case it is only potential vegetation in equilibrium with climate. (3) Because they are global or regional models (but not originally built for savannas), none of these models include *both* the particular relationships existing between trees and grasses that necessitate separate process treatment, *and* the proper definition of potential fuels in savannas. Similarly, the separation of savanna fuels into tree and grass components precludes the use of "big leaf" models that do not resolve productivity of trees and grasses separately. Finally, the need to capture fine sub-continental scale patterns of fuel load in the perspective of regional or continent fire emission estimates reduces the utility of full patch-scale models (for example, TREEGRASS model developed by Simioni and others (2000)).

This study presents a regional fuel load model developed to fulfill the aforementioned weak points including the use of a fine spatial resolution, specification of real vegetation through tree cover percentage, separate model physiological processes for trees and grass, proper potential evapotranspiration calculation in these tropical regions, and detailed characterization of surface fuel types. The model combines several advantages of each model group: it is based on a patch-scale production efficiency model (PEM) scaled up to the regional level using empirical relationships between patch-scale behavior and multi-source remote sensing data (spatio-temporal variability of vegetation, radiation, and climatic variables). In contrast to previous models where all available observations were used in the calibration and no field data were available to validate them (Potter and others 1993; Ruimy and others 1996), the present fuel load model has been calibrated from measurements recorded in 1996 along the Kalahari transect (Thomas and Shaw 1993; Dowty 1999; Woodward and Lomas 2004), and validated from independent site measurements recorded during the SAFARI 2000 dry season field campaign (Swap 2002), and other past campaigns.

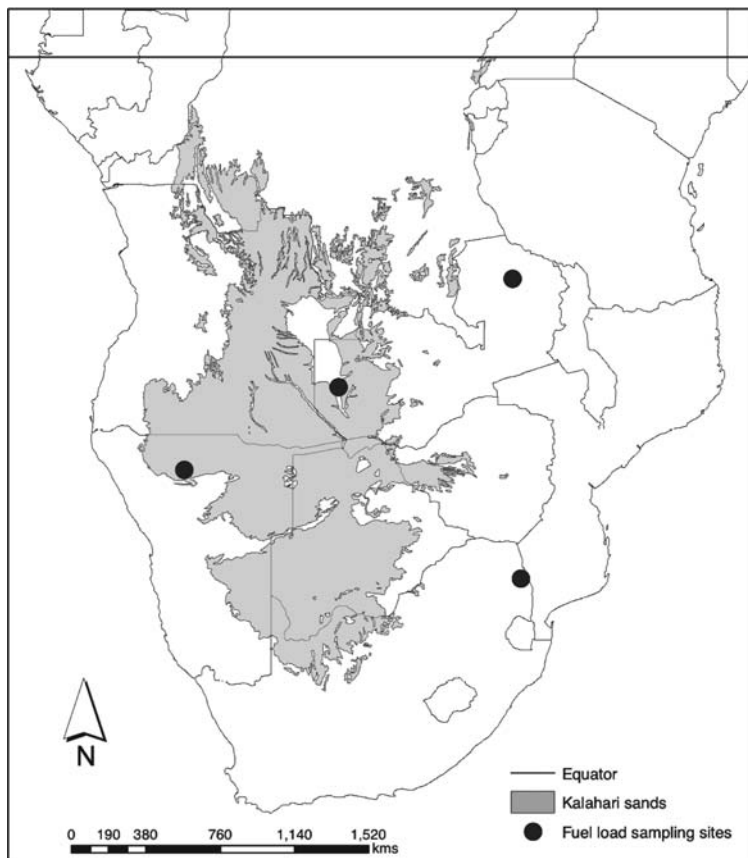


**Figure 1.** Southern equatorial African continent with the Kalahari sands and the four regions (Etosha—Namibia, Mongu and Kasama—Zambia, and Kruger National Park—Republic of Southern Africa) under focus.

The objectives of the study are threefold: (1) to present with maximum details the model processes and the associated temporal fuel allocation; (2) to test the model's sensitivity to input climate variables (precipitation, air temperature, and radiation) through a sensitivity analysis based on the 1999–2000 growing year; and (3) to explore the performance of the model by comparing predicted fuel loads with few available field measurements. With respect to objective two, our main hypothesis is that the model should be most sensitive to precipitation as water availability is considered to be the most limiting factor for productivity over southern African regions (Scholes and Walker 1993).

## MATERIAL AND METHODS

### Study Area

The study area encompasses the African continent south from the equator (Figure 1), which is mainly dominated by savannas ecosystems such as those occurring on Kalahari sands. This region was also the subject of an intensive wet season SAFARI 2000/Kalahari Transect ground campaign to characterize vegetation structure/composition and to

validate remote sensing of vegetation (Otter and others 2002). The Kalahari desert is an area of contiguous sand basins with a shared sedimentary history (Thomas and Shaw 1993). This region spans a strong and systematic precipitation gradient from the moist tropics to the arid sub-tropics. The Kalahari supports vegetation ranging from arid shrubland, the 'Kalahari Desert', through a gradient of savanna complexes to open, drought-deciduous Kalahari woodland and evergreen forest. Therefore, we use information collected along the Kalahari transect to capture model behavior across a strong natural rainfall gradient that is related to an equally strong gradient in vegetation structure. Model parameters have been based on data from field sites in the Kalahari (Scholes and others 2002; Caylor and others 2003; Caylor and others 2004; Scholes and others 2004).

### Outline of the Production Efficiency Model

To accommodate the southern African growing season, which occurs from October to May, the PEM simulations include twenty-four 15-day intervals from 1 September to 31 August of the

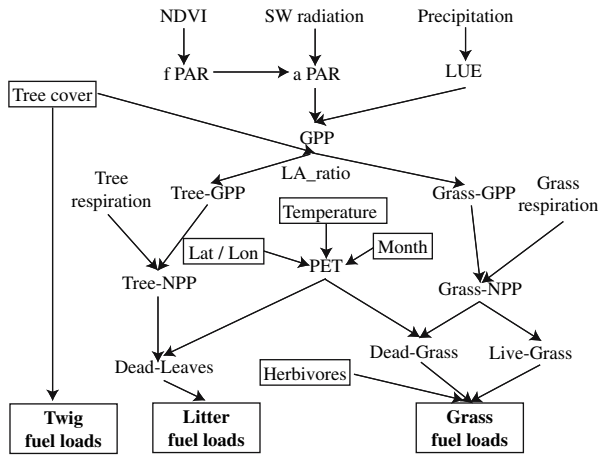


Figure 2. Components of the Fuel load—net primary production model. Input data are indicated with plain font in *rectangles*, processing steps without frame, and output data, namely the different fuel types, with *bold font in rectangles*.

following year. Leaf-out occurs when the NDVI records its maximum increase relative to the previous time step, and trees are assumed to produce their entire leaf area in one time step. The model is driven primarily by the absorption of photosynthetically active radiation (PAR) and light-use efficiency (LUE) (Figure 2). Light-use efficiency and PAR are used to determine gross primary production (GPP) in terms of grams of carbon per square meter over each 15-day simulation interval [ $\text{g-C m}^{-2} \text{15-day}^{-1}$ ], which is converted to biomass using a constant fractional carbon ratio of 0.45 (Scholes and Walker 1993). In each time step, GPP is partitioned into tree and grass components using the leaf area ratio between trees and grasses. The grass GPP is subsequently reduced to net primary production (NPP) by incorporating respiration costs. Tree NPP corresponding to non-leaf material is tracked but because non-leaf tree material is not part of the fuel load, non-leaf NPP is not reported here. Leaf fall is determined from a leaf stress ratio that compares the potential evapotranspiration (PET) to the cumulated precipitation over the time step. If PET is greater than precipitation, tree leaves and grass die proportionally to the stress ratio. Leaf fall increases the magnitude of the dead tree and grass leaf components of fuel load. Loads of live green and dead grass fuel types are also affected by herbivory, which reduces live grass preferentially over dead grass. Fuel load is resolved for each time step as live grass, dead grass, and tree leaf litter. Because live tree leaves are not considered as fuel, their loads are not presented. Small diameter twig

load is estimated empirically from the percent tree cover (Hansen and others 2000), using a relationship derived from SAFARI-92 data (Shea and others 1996; Trollope and others 1996), SAFARI 2000 field data, and additional field observations (R.J. Scholes pers. com. 2001). Therefore the amount of twigs varies spatially with tree cover, but is temporally constant, and represents the available load of twigs accumulated over several years between two fire occurrences.

## Model Input Variables

**Vegetation.** The spatial variability of savanna vegetation composition over the southern African region is represented by the University of Maryland 1 km<sup>2</sup> percent tree cover product (Hansen and others 2000). The temporal variability of vegetation productivity during the 1999–2000 growing season is captured by using 8-km resolution 15-day normalized difference vegetation index (NDVI) product processed by the NASA global inventory monitoring and modeling studies (GIMMS) group (Los and others 1994).

**Radiation.** Absorbed photosynthetically active radiation is used by the PEM to estimate GPP. Net downward surface shortwave radiation data set has been extracted from the NCEP/NCAR Reanalysis Monthly Means products (Kalnay and others 1996), and monthly values have been interpolated at  $0.5 \times 0.5$  and repeated twice a month to be in agreement with the temporal 15-day time step.

**Meteorological Variables.** Mean temperature and cumulative precipitation are needed biweekly to compute the light use efficiency (LUE) and PET. These variables were computed from 225 weather stations for the 1999–2000 period, using a preformatted daily subset of climate station data extracted from the national climatic data center (NCDC) Global Surface Summary of Day Data, Version 6 (Nickeson and others 2002). These data were interpolated biweekly over the southern Africa (0.5-degree pixel size resolution) using an inverse distance weighting method.

**Grazing Uptake.** Herbivory is an important factor that can reduce potential fuel load of dead and green grass by anywhere from 15 to 80% in unusually productive and nutritious ecosystems (van Wilgen and Scholes 1997; Scholes 1998). To account for the effect and spatial distribution of large herbivores (cattle and wildlife) on fuel load, a database from Peter de Leeuw (International Livestock Center for Africa personal com. 1999) is used. The model only takes into account herbivory for the grass layer because data concerning browsing is

sparse and the effect of browsing on fuel load is believed to be negligible (Scholes and Walker 1993). The Livestock Unit is set constant to 150 kg as in Scholes and others (1996).

## Model Routines

**Calculation of GPP.** The GPP calculation proceeds according to equations (1)–(4). Estimation of incident photosynthetically active radiation (PAR) ( $\text{J m}^{-2} \text{15-day}^{-1}$ ) follows Jones (1992), and is given in equation (1):

$$\text{PAR} = \sum_{i=1}^{15} (0.5 \times \downarrow \text{SW}_i) \quad (1)$$

where  $\downarrow \text{SW}_i$  is the total incoming shortwave radiation in  $\text{J day}^{-1}$ . The calculation of the fraction of photosynthetically active radiation absorbed by vegetation (fPAR) for each time step  $t$  and at each pixel  $[i,j]$  is determined from NDVI according to Prince and Goward (1995) and is shown in equation (2):

$$\text{fPAR}(t)_{[i,j]} = 1.67 \times \text{NDVI}(t)_{[i,j]} - 0.08. \quad (2)$$

Absorbed photosynthetically active radiation [ $\text{J m}^{-2} \text{15-day}^{-1}$ ] is then simply the product of fPAR and PAR, according to equation (3):

$$\text{APAR}(t)_{[i,j]} = \text{fPAR}(t)_{[i,j]} \times \text{PAR}(t)_{[i,j]}. \quad (3)$$

Gross primary productivity (GPP) ( $\text{g-C m}^{-2} \text{15-day}^{-1}$ ) is determined from equation (4):

$$\text{GPP}(t)_{[i,j]} = \text{LUE}(t)_{[i,j]} \times \text{APAR}(t)_{[i,j]}. \quad (4)$$

Light use efficiency (LUE) of the vegetation ( $\text{g-C MJ}^{-1} \text{PAR}$ ) is modeled as an empirical relationship derived from site-level modeling (Dowty 1999; Caylor and others 2004). The site-level model contains leaf physiology routines including models for  $\text{C}_3$  and  $\text{C}_4$  photosynthesis, stomatal conductance and  $\text{CO}_2$  and water diffusion through the stomata (Dowty 1999; Caylor and others 2004). All tree leaves were assumed to assimilate  $\text{CO}_2$  by the  $\text{C}_3$  photosynthetic pathway using the modified Farquhar and others (1980) equation (Woodward and others 1995), and all grasses by the  $\text{C}_4$  pathway (modified from Collatz and others (1992)). Our simulation results at the site scale show LUE to be strongly related to the weighted sum of the previous and current month's precipitation (40 and 60% weights, respectively).  $X_{\text{PRCP}}$  is the weighted

precipitation (PRCP) at pixel  $[i,j]$  during time  $t$  (equation (5)).

$$X_{\text{PRCP}} = 0.4 \times \text{PRCP}(t-1)_{i,j} + 0.6 \times \text{PRCP}(t)_{i,j}. \quad (5)$$

The patch-model relationship between LUE and precipitation tends to be linear up to a certain maximum threshold of precipitation above which LUE is maximum and constant (Figure 3). To approximate these two separate regimes of LUE response to weighted precipitation, the curve fitting approach used by Collatz and others (1992) is employed to find the smaller root of two separate functions (equations (6) and (7)). Equation (6) describes the linear "dry" regime of the LUE and precipitation response ( $f_1$ ), whereas equation (7) describes the constant "wet" regime where LUE is insensitive to changes in weighted precipitation ( $f_2$ ):

$$f_1 = A1_{\text{PRCP}} \times X_{\text{PRCP}} + A2_{\text{PRCP}} \quad (6)$$

$$f_2 = A3_{\text{PRCP}} \quad (7)$$

The parameters  $A1_{\text{PRCP}}$ ,  $A2_{\text{PRCP}}$  and  $A3_{\text{PRCP}}$  in equations (6) and (7) represent the best-fit parameters determined from 30,000 random simulations across the range of site-specific measured values. From these simulations and in the present study context, values for  $A1_{\text{PRCP}}$ ,  $A2_{\text{PRCP}}$  and  $A3_{\text{PRCP}}$  are 0.0138, 0.05, and 1.89, respectively. The approach of Collatz and others (1992) combines and smoothes the two separate functions, and then extracts LUE as being the smaller root of the quadratic equation. The resulting relationship describes the empirical relationship between weighted precipitation and LUE used in this study ( $R^2 = 0.83$ ;  $P < 0.001$ ;  $N = 120$ ).

$$\text{LUE}(t)_{i,j} = \frac{(f_1 + f_2) - \sqrt{(f_1 + f_2)^2 - 4(0.95 \times f_1 \times f_2)}}{2 \times 0.95} \quad (8)$$

where 0.95 is a coefficient indicating the level of co-limitation of the two functions.

**Tree/Grass Allocation of GPP.** The GPP is partitioned to tree and grass components based on the timing of the grass leaf-out calculated from the change in the NDVI values and the ratio of tree leaf area to grass leaf area. If the current time step is before the NDVI-detected grass leaf-out, all GPP is assigned to the tree component. If the current time step is after grass leaf-out, GPP is partitioned according to the ratio of tree leaf area to grass leaf

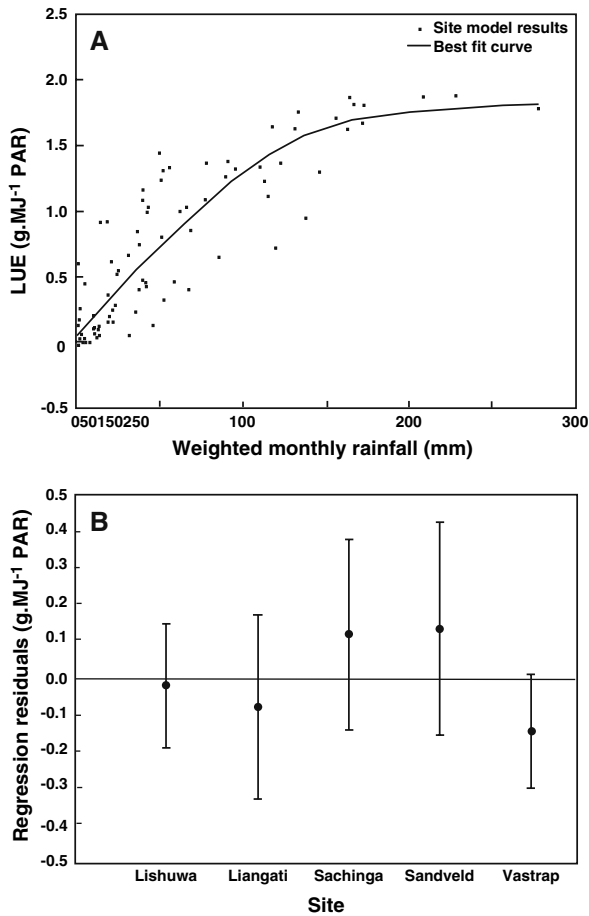


Figure 3. Derivation of the light use efficiency–precipitation relationship from field measurements in five sites located along the Kalahari transect. The tree cover percentage variable (TC) is implicitly included in the analysis as the five sites differ also from their TC value (from 58% in Lishuwa site located on the northern end of the transect to 5% in the southern Vastrap site). First, the three coefficients representing the parameters involved in  $y_1$  and  $y_2$  were derived for each of the five sites. Each parameter range was then derived from its minimum and maximum values reached along the Kalahari transect. Secondly, 30,000 runs of the combination and smoothing of  $y_1$  and  $y_2$  (following the Collatz and others (1992) approach), using random coefficient values within respective ranges were computed. The best fit, minimizing the sum of squares residuals is presented in (A) while the residual dispersions per site are reported in (B).

area. Field data at six sites from the Kalahari transect (Dowty 1999; Caylor and others 2004; Scanlon and Albertson 2004; Scholes and others 2004; Woodward and Lomas 2004) are used to parameterize a relationship between the ratio of tree/grass leaf areas and tree cover (Figure 4). Field grass leaf area values were determined from biomass measurements and specific leaf area at each site. Tree leaf area estimates were determined from stem map

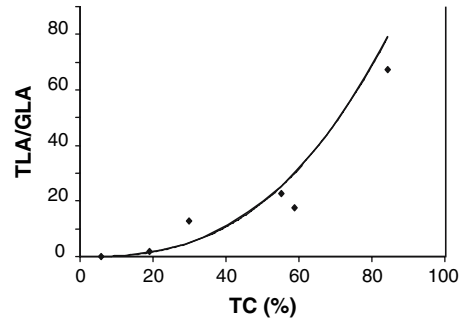


Figure 4. Change of the ratio between tree leaf area and grass leaf area along the tree cover gradient (%) based on field data collected along the Kalahari transect with  $n = 6$  and  $R^2 = 0.958$ .

data presented in Caylor and others (2003), wet season leaf mass allometry, and specific leaf area estimates taken from Goodman (1990). This relationship is then applied to the University of Maryland tree cover map to produce the leaf area ratio in each pixel. The parameterized function ( $R^2 = 0.96$ ;  $P < 0.005$ ;  $N = 6$ ) is given according to

$$LAR_{[i,j]} = \frac{TLA_{[i,j]}}{GLA_{[i,j]}} = 0.0006 \times (\text{TreeCover}_{[i,j]})^{2.6756} \quad (9)$$

where TLA is the tree leaf area, GLA is the grass leaf area (both in units  $\text{m}^2/\text{m}^2$ ), TreeCover is the percent woody vegetation cover (trees and shrubs), and LAR is the leaf area ratio. Equations (10) and (11) are used to allocate GPP into tree and grass components ( $\text{GPP}_{\text{TREE}}$  and  $\text{GPP}_{\text{GRASS}}$ , respectively)

$$\text{GPP}_{\text{TREE}}(t)_{[i,j]} = \text{GPP}(t)_{[i,j]} \times \left( \frac{LAR_{[i,j]}}{1 + LAR_{[i,j]}} \right) \quad (10)$$

$$\text{GPP}_{\text{GRASS}}(t)_{[i,j]} = \text{GPP}(t)_{[i,j]} - \text{GPP}_{\text{TREE}}(t)_{[i,j]} \quad (11)$$

*Tree Respiration and Net Primary Production (NPP).* Because our model focuses on fuels and tree GPP refers to the live woody compartment of trees, tree respiration and tree NPP calculations are not reported here. However, tree GPP is calculated to extract the grass GPP.

*Respiration and Net Primary Production of Grass.* The net primary production (NPP) of grass is calculated by subtracting respiration from GPP. Three distinct sources of respiration are taken into account—leaf respiration (dark respiration), non-leaf maintenance respiration (function of biomass), and synthesis respiration. Each of these respiration terms is calculated using equations and parameters

taken from the DOLY model (Woodward and others 1995). Total soil carbon is assumed to be 1,000 g m<sup>-2</sup>, and an air temperature of 25°C is used to represent the southern African environmental conditions along the Kalahari transect. All respiration terms are in units of g-C m<sup>-2</sup> 15-day<sup>-1</sup>.

**Leaf Respiration.** The leaf dark respiration (Rleaf) is based on the quantity of carbon in green grass. This carbon amount depends on the mean specific leaf area for live grass estimated from samples collected on the Kalahari transect (2 m<sup>2</sup> kg<sup>-1</sup> from Dowty (1999)). Equation (12) is used to determine Rleaf for grasses

$$R_{\text{leafGRASS}}(t)_{[i,j]} = \kappa \times p \times \frac{12g - C}{\text{mol}} \times \text{LAI}_{\text{GRASS}}(t)_{[i,j]} \quad (12)$$

where  $\kappa$  is the respiration rate (Woodward and others 1995), and  $p$  a time constant

$$\kappa = \frac{2 \times 10^{-6} \text{mol} - C}{\text{m}^2 \text{s}} \quad (13)$$

$$p = \frac{1,296,000 \text{s}}{15 \text{days}} \quad (14)$$

**Non-Leaf Maintenance Respiration.** The non-leaf maintenance respiration equation is based on Woodward and others (1995). The calculation of grass non-leaf maintenance respiration (Rmaint<sub>GRASS</sub>) is estimated using the belowground biomass, which is assumed to be 0.5 of the total grass biomass

$$R_{\text{maintGRASS}}(t)_{[i,j]} = 0.5 \times M_{\text{GRASS}}(t)_{[i,j]} \times \frac{K_M}{24} \times e^{-0.0504} \quad (15)$$

Where  $K_M$  is equal to 0.7 (y<sup>-1</sup>) and is the constant of proportionality for dependence of maintenance respiration on tissue mass during the year.

**Synthesis Respiration.** The residual production from the maintenance respirations is available for producing biomass and is subject to synthesis respiration according to equation (16)

$$R_{\text{synthGRASS}}(t)_{[i,j]} = \left[ GPP_{\text{GRASS}}(t)_{[i,j]} - R_{\text{leafGRASS}}(t)_{[i,j]} - R_{\text{maintGRASS}}(t)_{[i,j]} \right] \times \frac{K_S}{1 + K_S} \quad (16)$$

The constant of proportionality for the dependence of synthesis respiration on the mass of new tissue synthesized ( $K_S$ ) is set constant at 0.3 (g/g). Finally, the NPP<sub>GRASS</sub> results from the difference between

the GPP and the expenditures from the three respiration types (equation (17)):

$$\begin{aligned} \text{NPP}_{\text{GRASS}}(t)_{[i,j]} = & GPP_{\text{GRASS}}(t)_{[i,j]} - \left( R_{\text{leafGRASS}}(t)_{[i,j]} \right. \\ & \left. + R_{\text{maintGRASS}}(t)_{[i,j]} + R_{\text{synthGRASS}}(t)_{[i,j]} \right) \end{aligned} \quad (17)$$

**Leaf Death, and Litter Fall.** The amount of green leaves (both trees and grass) that die during each time step ( $t$ ) in a given pixel  $[i,j]$  depends on the index of water availability (Field and others 1995; Scholes and others 1996). This index is assessed by calculating the Thornthwaite potential evapotranspiration (PET<sub>Thorn</sub>) (mm 15-day<sup>-1</sup>) (Thornthwaite 1948), which is corrected using annual precipitation and annual Penman PET (PET<sub>Penman</sub>) (mm y<sup>-1</sup>) (UEA/CRU 1990). Such correction prevents an underestimation of PET in dry and semi-arid regions. The index of water availability ( $\omega$ ) is the ratio of precipitation to PET, and it is calculated for each time step. When  $\omega(t)$  is equal to or greater than 1 (PRCP  $\geq$  PET) there is no water stress and therefore no material death for either trees or grasses (equation (18)). In this case,  $\omega(t) = 0$ , and the NPP of the current time step is added to the previous time step. When  $\omega(t)$  is less than 1, death rate varies between trees and grasses according to equation (19)

$$\omega(t)_{[i,j]} \geq 1 \quad f_{\text{DeadGRASS}} = f_{\text{DeadTREE}} = 0 \quad (18)$$

$$\omega(t)_{[i,j]} < 1 \quad \begin{cases} f_{\text{DeadGRASS}} = 1 - \omega(t)_{[i,j]} \\ f_{\text{DeadTREE}} = \sum_{\tau=t}^{\tau=t^*} \left( \frac{1 - \omega(\tau)_{[i,j]}}{d_{\text{TREE}}} \cdot \frac{1}{(t - \tau) + 1} \right) \end{cases} \quad (19)$$

where  $f_{\text{DeadTREE}}$  and  $f_{\text{DeadGRASS}}$  are the fraction of dead leaf material accumulated during time-step  $t$  at pixel  $[i,j]$ . When  $\omega(t)$  is less than 1 for grasses, leaf death is directly proportional to the  $\omega(t)$ , and ranges from 0 (no leaf death) to 1 (total leaf death). For trees, the fraction of leaf death is found using a weighted cumulative water stress over the period of time  $t$  to  $t^*$ , with  $t^*$  representing the last period of time during which  $\omega(t)$  is greater than or equal to 1.  $d_{\text{TREE}}$  is set to 4 and limits the maximum fraction of leaf death to 0.25 for any single time step. With this assumption, at least 99% of all tree leaves will be killed 2 months after the beginning of any period without rainfall (that is, the end of the wet season). The amount of dead material produced during the current time step is added to the litter fuel load for

the dead tree leaves, and to the dead grass compartment for the dying grass.

**Herbivory and Fuel Load Allocations.** In the model, grass (both green and dead) is affected by grazing using herbivory data wherever it is available. For a given location, we assume that the amount of grass depleted by grazing is evenly distributed between months, and depends on the number of livestock units (LSU), with the conversion of different herbivore types into a single standard LSU. Grazed material is first removed from the green grass. If the predicted grazing needs are unsatisfied, the remainder is removed from the dead grass compartment. Calculation of the total amount of forage required by herbivores,  $F_{\text{TOTAL}}$  ( $\text{g-C m}^{-2} \text{ 15-days}^{-1}$ ) is based on the total energy demand by herbivores ( $E_{\text{TOTAL}}$ ) over a 15-day period ( $\text{MJ m}^{-2} \text{ 15-days}^{-1}$ ) defined as (Scholes and others 1996):

$$E_{\text{TOTAL}} = 0.4 \times (M_{\text{LSU}})^{0.84} \times N_{\text{LSU}} \times 15 \quad (20)$$

Where  $M_{\text{LSU}}$  is the mean mass of a livestock unit ( $150 \times 10^3 \text{ g}$ ) and  $N_{\text{LSU}}$  is the number of livestock units per square meter. The total forage required then depends on the grass digestibility, the grass energy content, and the grass carbon fraction according to:

$$F_{\text{TOTAL}} = \frac{\text{Cfrac}_{\text{GRASS}} \times E_{\text{TOTAL}}}{G_{\text{DIGEST}} \times G_{\text{ENERGY}}} \quad (21)$$

With the grass carbon fraction ( $\text{Cfrac}_{\text{GRASS}}$ ) set to 0.45, the grass digestibility ( $G_{\text{DIGEST}}$ ) to 60%, and the grass energy content ( $G_{\text{ENERGY}}$ ) to  $0.018 \text{ MJ g}^{-1}$  (Scholes and others 1996). If the green grass amount is less than the total forage required, herbivores will consume all the green grass and complete their requirement by consuming some dead grass. Here we assume that digestibility, energy content, and grass-carbon-fraction of dead grass is the same as for the green grass.

At the end of each time step and for every pixel, the model adds the current step increment of each component to that of the previous time step. Therefore, four different maps covering the southern African region are simultaneously produced at each time step. Each map presents the current accumulated load of one of the following fuel types: (1) live grass, (2) dead grass, (3) litter as dead tree leaves, and (4) live tree leaves. This last component is not really considered as fuel if a fire would occur because southern African fires are mainly surface fires that do not involve live tree

leaves. The model also produces a yearly map of the load of small woody debris that has fallen to the ground.

## Sensitivity Analyses

The sensitivity of the model in relation to the climate is tested through four scenarios of 1999–2000 climatic data (Observed, Southern African Mean, Mean + one Standard Deviation, and Mean – one Standard Deviation values). These scenarios were tested over Etosha and Kasama because these regions are the driest and wettest regions within the Kalahari transect, respectively. For a given simulation, two variables are set to the “values” determined for each site and the third variable is assigned the value averaged biweekly from the entire study region. Results are presented as anomalies from the “true” data, and are given for locations with 28 and 32% tree cover for Etosha and Kasama, respectively.

The sensitivity of the model related to the vegetation is also tested by conducting simulations under three different tree cover values—5, 30, and 50%—for several locations across the Kalahari transect. For these vegetation structure analyses, all the climatic data are set to means computed biweekly over the entire study area.

## Simulated versus Observed Fuel Loads

Fuel load simulations are conducted in the four regions where field measurements are available and for three different tree cover percentages (5, 30, and 50% at each site except Etosha, where maximum tree cover percentage is 33% in the park region). In a given region, sites with different tree cover percentages are selected from locations less than 10 km apart. Simulated fuel loads using the 1999–2000 observed biweekly climatic conditions are compared with field measurements from different field campaigns such as the SAFARI 2000 dry season field campaign when available (Hély and others 2003a; Alleaume and others 2005), as well as from the SAFARI-92 campaign (Shea and others 1996), and with unpublished data (R.J. Scholes pers. com. 2001).

## RESULTS

Figures 5 and 6 provide the spatial distribution of green and dead grass loads, respectively, over southern Africa for the whole year of simulation. Green grass begins to grow in November with slightly higher growth rates in the northwestern

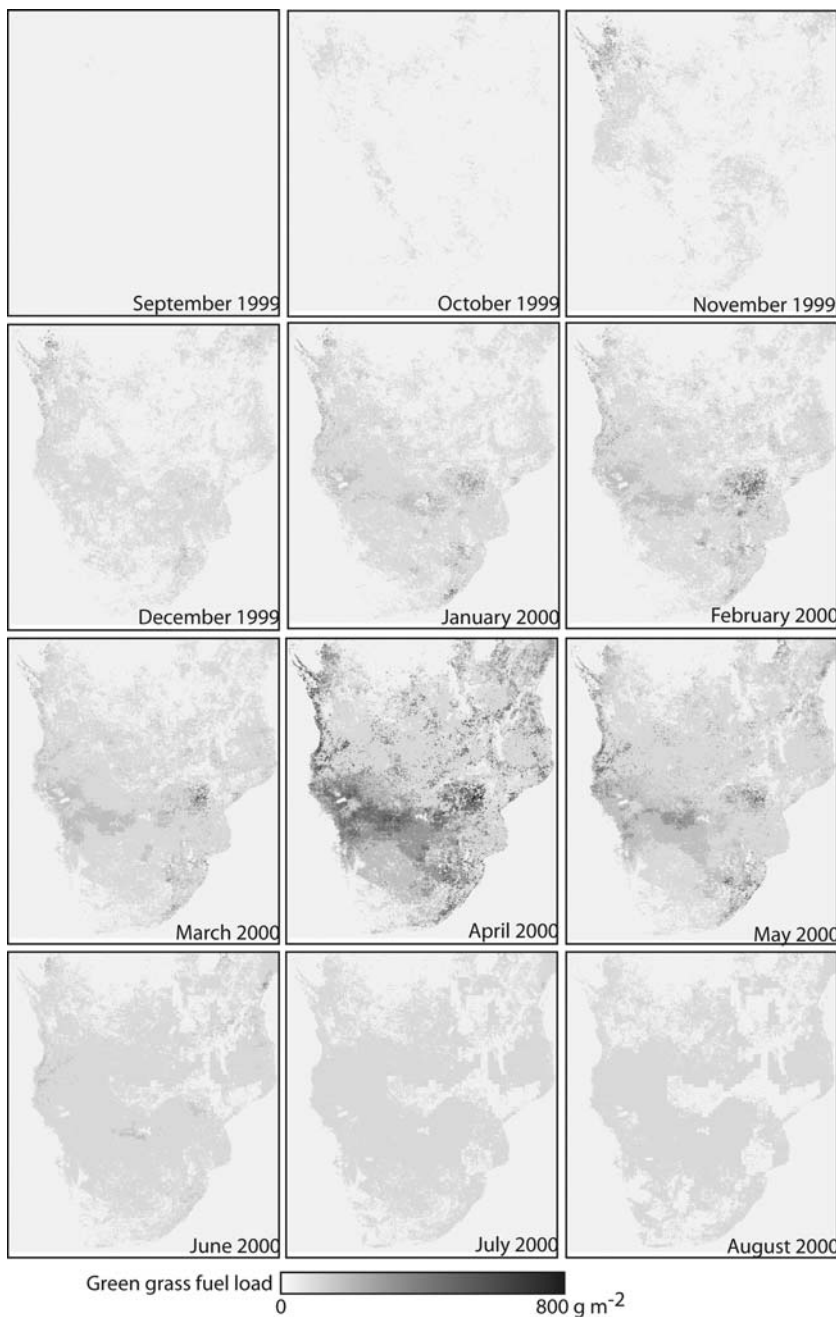


Figure 5. Spatial and temporal change in green grass fuel load over the Southern African region from September 1999 to August 2000, with April 2000 being the month of maximum production before decay.

region of the study area near the equator. From January until March, greater green grass loads are located in the Miombo region of Zimbabwe, Zambia and Angola. The entire study area is greenest in April, with the maximum green grass loads still being located in the Miombo region (ca.  $800 \text{ g m}^{-2}$ ). Thereafter, green grass is reduced over all of southern Africa by water stress, which causes increases in the amount of dead grass. Dead grass fuel loads increase continuously all over the year up to  $1,600 \text{ g m}^{-2}$  in the aforementioned Miombo region and southward in Botswana

(Figure 6). In regions where the herbivory pressure is important, both green and dead grasses are depleted. Near the equator, grass loads are quite light as compared to the Miombo because the region is mainly dominated by forests (tree cover mode is 80% over the region spanning from the equator to 5° South). In these heavily forested areas, the model predicts early growth of tree leaves up to  $419 \text{ g m}^{-2}$  in September, although this canopy leaf production is not considered to be potential fuel in surface fires. Figure 7 depicts the temporal changes in the fuel load components at

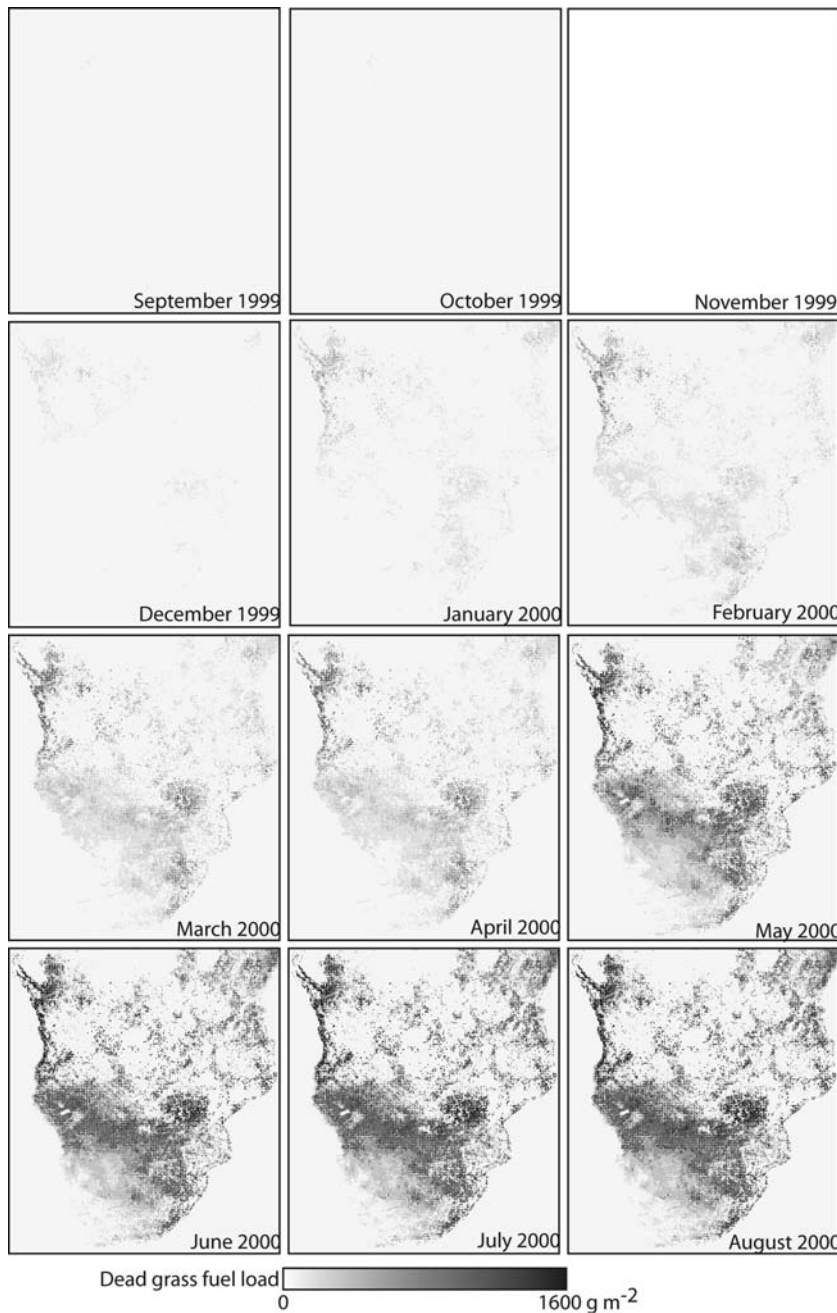


Figure 6. Spatial and temporal change in dead grass fuel loads over the Southern African region from September 1999 to August 2000, with heaviest accumulated dead grass loads in the Miombo region.

Etosha and Kasama, which exhibit the same general trends seen in Figure 6.

### Sensitivity Analyses

In both Etosha and Kasama, precipitation is the climate variable most influential in determining all fuel type productions (maximum anomaly variability in Figures 8 and 9, for Etosha and Kasama, respectively). Above-average precipitation leads to a tenfold increase in early season grass production at Kasama and a fivefold increase in grass produc-

tion at the end of the growing season in Etosha. In addition, greater precipitation leads to a longer growing season that may start up to 2 months earlier and may end 1 month later. Higher levels of grass production also cause greater amounts of dead grass, however the conversion from live to dead grass biomass is delayed. Finally, increases in precipitation lead to almost 50% less tree leaf litter and delays in the occurrence of tree leaf litter fall. Conversely, lower than average precipitation leads to lower grass production and a shorter growing season, which yields a reduced dead grass load that

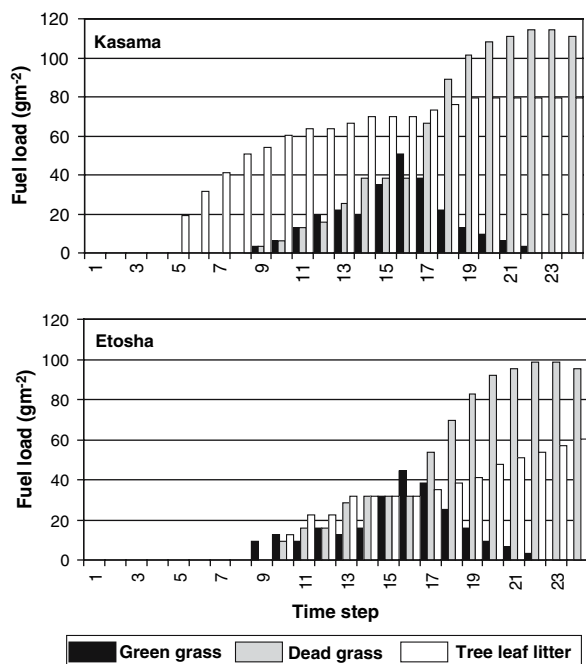


Figure 7. Temporal fuel load changes in terms of green grass, dead grass and tree leaf litter under observed climatic data for Etosha and Kasama sites with 28 and 32% of tree cover, respectively.

occurs earlier in the year. The reduction in precipitation also causes tree leaves to die earlier than with average precipitation.

Although precipitation has the greatest impact on fuel load predictions, the second most important climate variable affecting fuel types is radiation. Although changes in radiation do not impact predictions of tree leaf litter, increases in radiation at Kasama lead to 3 times larger grass fuel loads (both green and dead), whereas a decrease in radiation reduces the amount of grass by 50% in Etosha. Finally, temperature only slightly affects the predictions of total fuel load.

Under similar climate conditions, differences among sites within a region result from varying tree cover percentages. Our model predicts patterns of fuel load consistent with field observations: greater tree cover percentages lead to reduced total grass load (both live and dead), greater total tree leaf loads, and delayed onset of grass growth (Figure 10). Differences among regions are due to differences in NDVI, and the variability in fuel load associated with changes in tree cover and structural heterogeneity. In arid regions such as Etosha and Kruger, NPP does not become significant until December, which corresponds to an accumulated precipitation amount of 200 mm. In moister regions such as Mongu or Kasama, growth starts as

early as October when only 80–40 mm of rain has already fallen, respectively.

### Simulated Versus Observed Fuel Loads

Figure 11 provides the simulated and observed fuel loads at two different times within the 1999–2000 growing season. Except for fuel loads measured in 2000 at Kruger sites with trees, all the other measured data for August 2000 are within the simulated range for this same year (Figure 11, dots). A comparison between the simulated loads and independent field data from different years (Figure 11, crosses) reveals that both the composition and amount of fuel load are highly variable across southern Africa. Most temporal variation in fuel load throughout the fire season (May–August) is due to grass mortality, whereas tree litterfall does not vary much at all.

### DISCUSSION

We assess the performance of our regional fuel load model with respect to four different considerations: (1) the model's ability to simulate physiological and ecological processes representative of savannas, (2) the model's sensitivity to input factors, (3) the model's agreement with field measurements, and (4) the improvement in NPP modeling compared to other NPP models.

#### PEM Ability to Simulate the Physiological and Ecological Processes

In the present production efficiency model, the timing of many physiological processes is controlled by the NDVI time series. For instance, NDVI is explicitly used to define particular phenological events such as grass leaf emergence. If grass leaf emergence has not occurred, all simulated production is allocated to trees. However, as soon as leaf-out occurs, GPP is allocated to both tree and grass compartments. The 8 km resolution 15-day time step for NDVI is sufficient to capture leaf-out and leaf death after the rainy season, however a shorter time step and a finer spatial resolution is necessary to determine responses to individual rainfall events. However, higher resolution rainfall data is a limiting factor in improving the water use efficiency component of our PEM model because southern African precipitation is highly convective, leading to patchy distribution of rainfall in time and space (Scholes and Walker 1993).

Because savanna ecosystems are water-limited, the PEM tracks water stress both in the light use efficiency (LUE) calculation, and through the

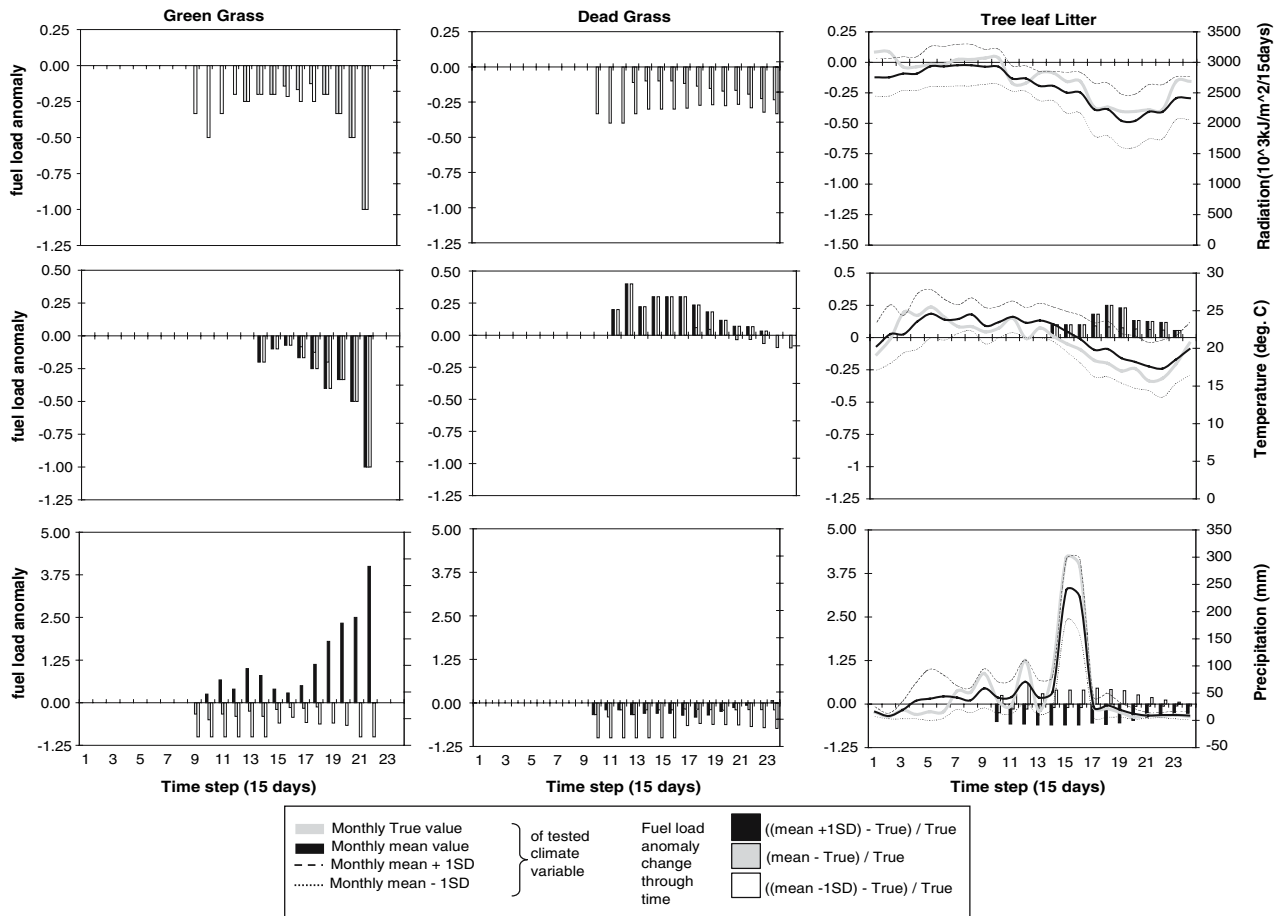


**Figure 8.** Temporal fuel load anomalies at Etosha (28% of tree cover). Radiation, temperature, and precipitation are the three climatic variables tested in the sensitivity analysis. For each test, one of these variables varies from the Mean – 1SD Dev (mean–) towards Mean, observed data (True), and Mean + 1SD Dev (mean+), while the two other variables are left equal to observed values. For each test, the biweekly values of the three fuel type loads, namely green and dead grass, and tree leaf litter are provided from 1 September onwards. Anomalies are computed as the ratio of the difference between load produced under the tested climate scenario and load produced under observed climate over load produced under that same observed climate.

process of leaf death via the potential evapotranspiration calculation. Although LUE is primarily a function of rainfall (equations (5)–(8)), we expect that the structural configuration and composition of landscapes will also have a secondary affect on LUE. Figure 2b presents the residuals of our empirical LUE function derived from the patch-scale model. The error within the overall LUE relationship is not normally distributed across sites, suggesting the need to formulate LUE relationships that consider tree cover and/or land cover. To improve our estimation of water stress, and to conform with FAO guidelines for arid regions (Allen and others 1998), we have implemented the Thornthwaite PET calculation with the annual Penman-Montheith PET and annual precipitation correction as suggested by the CRU/UEA research

team for arid and semi-arid regions (Crutzen and Andreae 1990; UEA/CRU 1990; Scholes and Walker 1993). As temperature and precipitation are involved in PET estimates, improved records in terms of spatial and temporal resolution would be useful as well. The lack of data on fine woody production in the tropical savanna ecosystems (Malaisse and others 1975) required the development of a simple twig load production based on a regional empirical relationship involving only the tree cover percentage. However, these loads reflect multi-year production so their accuracy is dependent on knowledge of the history of fire across the study region. As regional fire climatology within southern Africa is better understood, we expect estimates of woody contributions to fuel load to improve. The release of a global livestock database

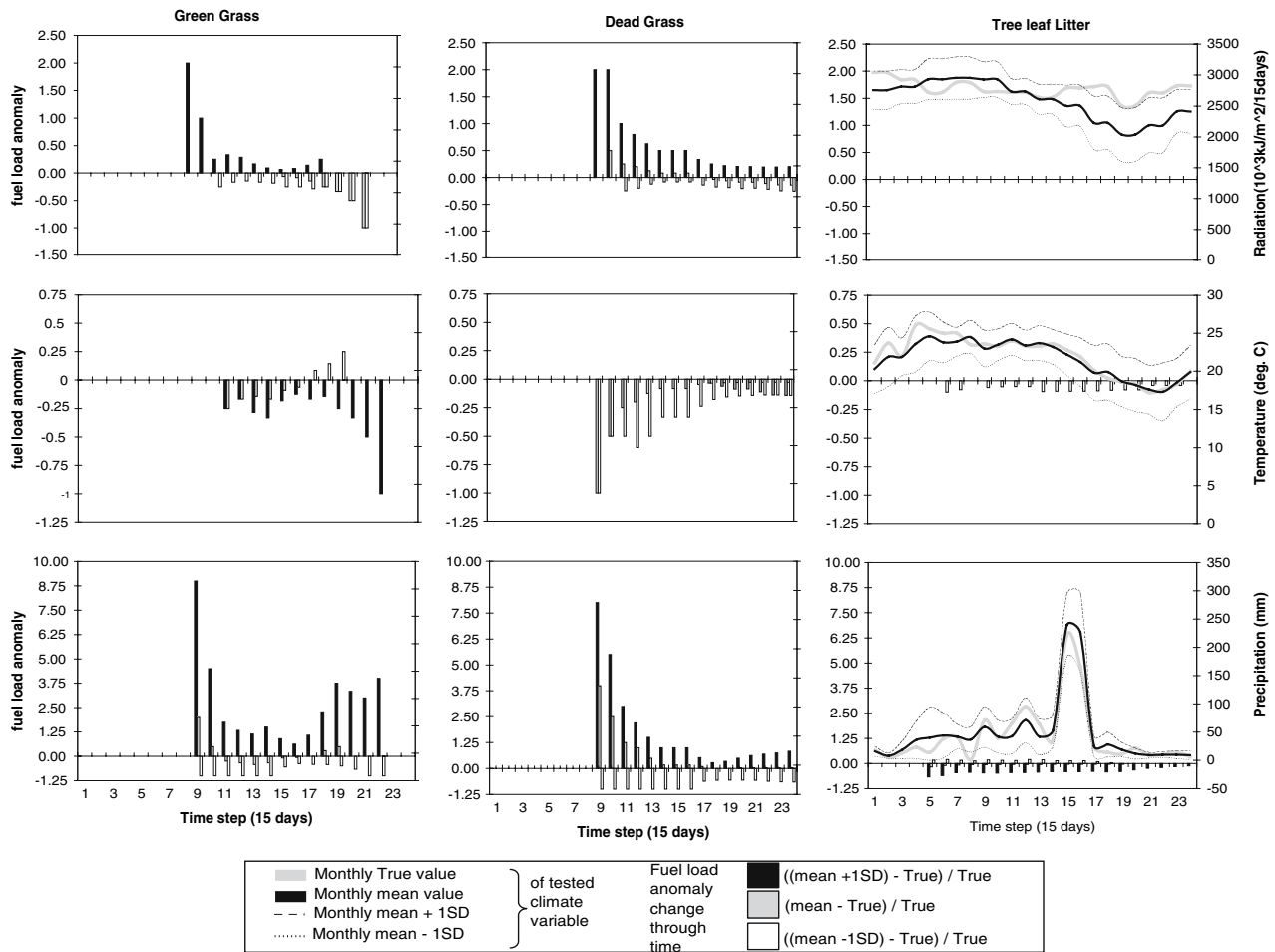


Figure 9. Temporal fuel load anomalies at Kasama (32% of tree cover), using the same presentation as in Figure 8.

(Pender and others 2001) will help clarify the role of herbivory in determining fuel load over southern Africa. Furthermore, the role of litter decomposers such as termites may be locally important, but no regional dataset on their distribution is currently available.

### PEM Sensitivity to Input Factors

Sensitivity analysis has confirmed the hypothesis that variability in precipitation is the most important climatic determinant of fuel load production. Precipitation used as input in the PEM should therefore present the most accurate spatial and temporal coverage possible. This could be realized by coupling higher resolution ground data to remotely sensed data such as the Tropical Rainfall Measuring Mission data set (Simpson and others 1988), which provides both precipitation and air temperature. We found that relatively cool temperatures at the end of the rainy season delayed

grass and tree leaf mortality up to 3 months. These trends in the input influences were also confirmed from an earlier 1991–1992 year simulation (Hély and others 2003b). The sensitivity of the model to NDVI has not been explicitly tested here although the spatial and temporal resolution of NDVI is clearly a critical limitation to the model’s ability to generate detailed fuel load patterns (less than 8 km). The new GIMMS-10 day NDVI composition procedure could increase temporal resolution, and the 500 m MODIS vegetation continuous fields (Hansen and others 2003) would better capture the spatial heterogeneity that is characteristic of these savanna ecosystems.

### Predictions Versus Field Measurements

The level of agreement between simulated fuel load and our independent fuel load observations seems satisfactory considering the high variability of precipitation in space and time, and the fact that pre-

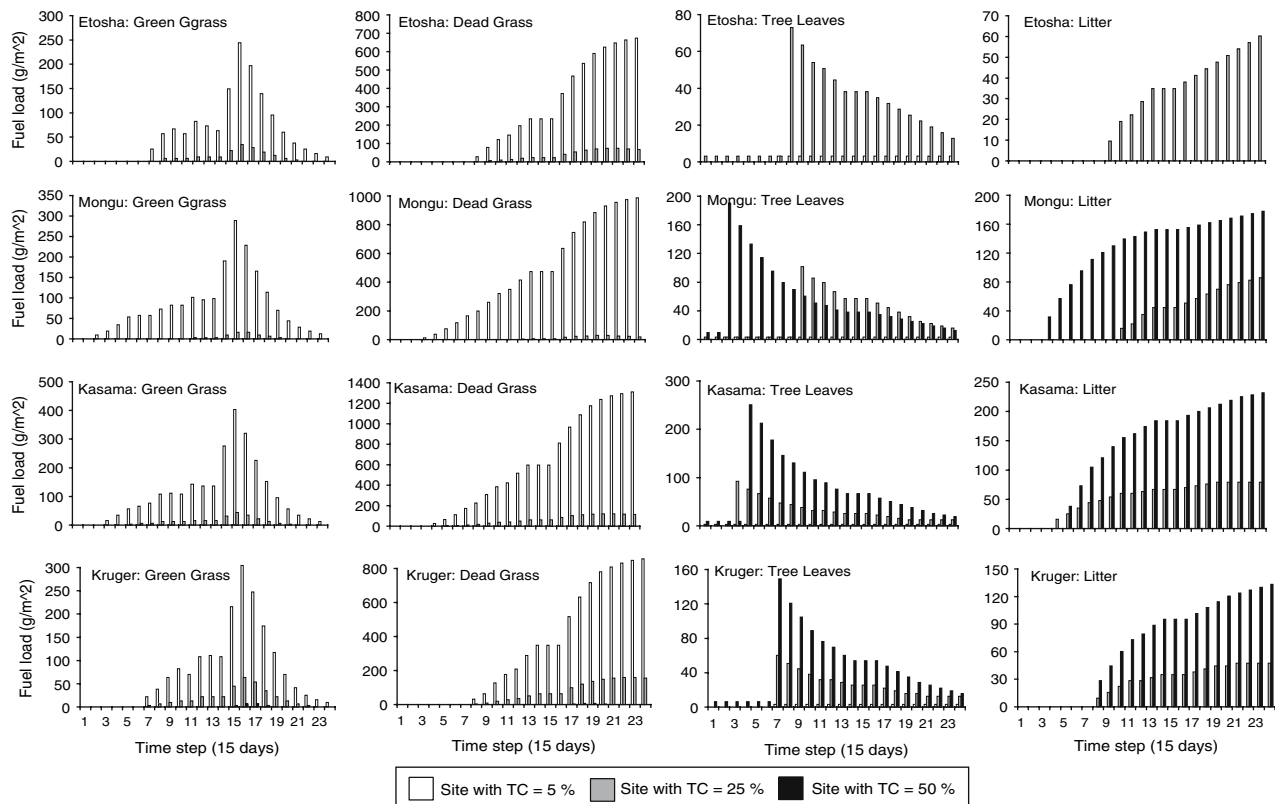


Figure 10. Impact of shift in percent tree cover on fuel production at Etosha, Mongu, Kasama, and Kruger regions. Tree cover varies from 5 to 50%. For all four regions, biweekly climatic values are set to the mean value across southern Africa.

viously published data are not always specific about the exact tree cover percentage of the studied site (Shea and others 1996; Trollope and others 1996). In addition, sampling bias in field measurements may influence the fuel load estimation. For instance, the Kruger grass loads in 2000 (T. Landmann pers. com. 2002) were estimated from the disc pasture method (Trollope and others 1996), but it has been recognized that this method may be less accurate when grass is sparse such as semi-arid savannas or in stands with relatively high tree cover. Furthermore, data from Kruger seem to demonstrate high variability in observed fuel loads (compare Figure 11).

### Comparison of the Fuel Load PEM with Other NPP Models

As compared to other models used to estimate NPP, our approach combines a number of specific advantages, and also addresses several issues identified by previous studies. The 1-km UMD tree cover map is the finest spatial scale ever used in global or regional NPP models, and also describes the actual vegetation patterns that reflect the result

of human activities (for example, deforestation and bush encroachment). Semi-monthly NDVI averages provide a reasonably short time step to capture the change in fuel production and quality through the dry season (Hoffa and others 1999). Our model has specifically been developed for savanna ecosystems to accommodate the biophysical and structural differences between trees and grasses demonstrated by previous studies (Goetz and others 1999; Simioni and others 2000; van der Werf and others 2003). In addition, our model also resolves fuel load into separate fuel types. Because large diameter woody debris (trunk and branches) are not involved in the propagation of surface fires in savannas, we do not report this fuel type in the present model.

In the context of global change and the impact of biomass burning worldwide, our fuel load model provides estimates in time and space in such a way that uncertainties related to biomass available for fire propagation should be better constrained. Moreover, coupled to monthly or higher frequency burned area products, such fuel load estimates should also be valuable to reduce uncertainties in carbonaceous compound emissions.

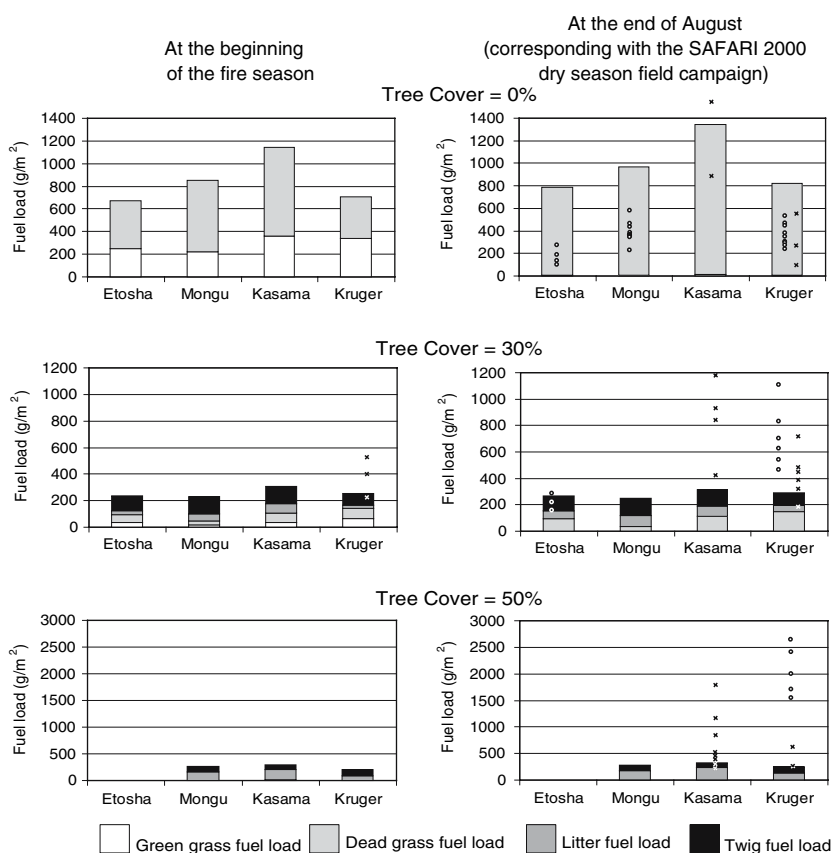


Figure 11. Total fuel loads and their composition in May and August (beginning and mid-fire season, respectively) in Etosha, Mongu, Kasama, and Kruger regions for three different tree cover: 0, 30, and 50%. Histograms represent simulated loads under the current climatic condition in 1999–2000. Dots represent values measured during the SAFARI 2000 dry season field campaign in Mongu (Hély and others 2003a); Alleaume and others (2005) for Etosha; T. Landmann, pers. comm. for Kruger), whereas crosses represent values ever recorded in these regions with similar tree cover percentages (Shea and others (1996); R.J. Scholes, pers. comm., T. Landmann, pers. comm., Hély, unpublished data).

## ACKNOWLEDGEMENTS

This paper is part of the SAFARI 2000 “Southern African Regional Science Initiative”. This research has been supported by the Southern Africa Validation of EOS program (SAVE– NASA-NAG5-7266), and the Interdisciplinary Science program (IDS-NASA-NAG5-9357). We thank Simon Brewer for assisting with model programming, Jaime Nickeson, Compton J. Tucker, the Global Inventory Monitoring and Modeling Studies for the NDVI data sets, and the Data Assimilation Office (DAO) at the Goddard Space Flight Center’s Distributed Active Archive Center (DAAC) for the climatic data, and the NOAA/OAR/ESRL PSD, Boulder, Colorado, USA, for the NCEP Reanalysis Derived data (Web site at <http://www.cdc.noaa.gov/>).

## REFERENCES

- Alleaume S, Hély C, Le Roux J, Korontzi S, Swap RJ, Shugart HH, Justice CO. 2005. Using MODIS to evaluate heterogeneity of biomass burning in southern African savannahs: a case study in Etosha. *Int J Remote Sens* 26:4219–37.
- Allen RG, Pereira LS, Raes D, Smith M. 1998. Crop evapotranspiration—guidelines for computing crop water requirements. FAO Irrigation and drainage paper 56, Rome.
- Atjay GL, Ketner P, Duvigneaud P. 1987. Terrestrial primary production and phytomass. In: Bolin B, Ed. *The global carbon cycle*. New York: Wiley. pp 129–81.
- Caylor KK, Shugart HH, Dowty PR, Smith TM. 2003. Tree spacing across the Kalahari transect in southern Africa. *J Arid Environ* 54:281–96.
- Caylor KK, Dowty PR, Shugart HH, Ringrose S. 2004. Relationship between small-scale structural variability and simulated vegetation productivity across a regional moisture gradient in southern Africa. *Global Change Biol* 10:374–82.
- Collatz GJ, Ribascarbo M, Berry JA. 1992. Coupled photosynthesis-stomatal conductance model for leaves of C4 plants. *Aust J Plant Physiol* 19:519–38.
- Cramer W, Kicklighter DW, Bondeau A, Moore III B, Churkina G, Nemry B, Ruimy A, Schloss AL, Participants of “Postdam’95”. 1999. Comparing global models of terrestrial net primary productivity (NPP): overview and key results. *Global Change Biol* 5(Suppl 1):1–15DOI: 10.1046/j.1365-2486.1999.00009.x.
- Crutzen PJ, Andreae MO. 1990. Biomass burning in the tropics: impact on atmospheric chemistry and biogeochemical cycles. *Sci New Ser* 250:1669–78.
- Delmas RA, Loudjani P, Podaire A, Menaut JC. 1991. Biomass burning in Africa: an assessment of annually burned biomass. In: Levine JS, Eds. *Global biomass burning: atmospheric, climatic, and biospheric implications*. Cambridge: MIT Press. pp 126–32.
- Desanker PV, Frost PGH, Justice CO, Scholes RJ. 1997. The Miombo network: framework for a terrestrial transect study of land-use and land-cover change in the Miombo ecosystems of

- Central Africa: conclusion of the Miombo network workshop. IGBP report 41, The International Geosphere-Biosphere Programme, Stockholm.
- Dowty PR. 1999. Modeling biophysical processes in the savannas of southern Africa. Ph.D. thesis. University of Virginia, Charlottesville.
- Dwyer E, Pinnock S, Gregoire JM, Pereira JMC. 2000. Global spatial and temporal distribution of vegetation fire as determined from satellite observations. *Int J Remote Sens* 21:1289–302.
- Farquhar GD, von Caemmerer S, Berry JA. 1980. A biochemical model of photosynthetic CO<sub>2</sub> assimilation in leaves of C<sub>3</sub> plants. *Planta* 149:78–90.
- Field CB, Randerson JT, Malmström CM. 1995. Global net primary production: Combining ecology and remote sensing. *Remote Sens Environ* 51:74–88.
- Goetz SJ, Prince SD, Goward SN, Thawley MM, Small J. 1999. Satellite remote sensing of primary production: an improved production efficiency modeling approach. *Ecol Model* 122:239–55.
- Goodman PS. 1990. Soil, vegetation and large herbivore relations in Mkizi game reserve, Natal. Ph.D. thesis. University of the Witwatersrand, Johannesburg.
- Hansen MC, DeFries R, Townshend JRG, Carroll M, Dimiceli C, Sohlberg R. 2003. Global percent tree cover at a spatial resolution of 500 meters: first results of the MODIS vegetation continuous fields algorithm. *Earth Interact* 7:1–15.
- Hansen MC, Defries RS, Townshend JRG, Sohlberg R. 2000. Global land cover classification at 1km spatial resolution using a classification tree approach. *Int J Remote Sens* 21:1331–64.
- Haxeltine A, Prentice IC. 1996. BIOME3: an equilibrium terrestrial biosphere model based on ecophysiological constraints, resource availability, and competition among plant functional types. *Global Biogeochem Cycles* 10:693–709.
- Hély C, Alleaume S, Swap RJ, Shugart HH, Justice CO. 2003. SAFARI-2000 characterization of fuels, fire behavior, combustion completeness, and emissions from experimental burns in infertile grass savannas in western Zambia. *J Arid Environ* 54:381–94.
- Hély C, Dowty PR, Alleaume S, Caylor K, Korontzi S, Swap RJ, Shugart HH, Justice CO. 2003. Regional fuel load for two climatically contrasting years in southern Africa. *J Geophys Res* 108:8475.
- Hoffa EA, Ward DE, Hao WM, Susott RA, Wakimoto RH. 1999. Seasonality of carbon emissions from biomass burning in a Zambian savanna. *J Geophys Res* 104:13841–53.
- Hunt ER, Piper SC, Nemani R, Keeling CD, Otto RD, Running SW. 1996. Global net carbon exchange and intra-annual atmospheric CO<sub>2</sub> concentrations predicted by an ecosystem process model and three-dimensional atmospheric transport model. *Global Biogeochem Cycles* 10:431–56.
- Jones HG. 1992. Plants and microclimate: a quantitative approach to environmental plant physiology. Cambridge: Cambridge University Press.
- Kalnay E, Kanamitsu M, Kistler R, Collins W, Deaven D, Gandin L, Iredell M, Saha S, White G, Woollen J, Zhu Y, Chelliah M, Ebisuzaki W, Higgins W, Janowiak J, Mo KC, Ropelewski C, Wang J, Leetmaa A, Reynolds R, Jenne R, Joseph D. 1996. The NCEP/NCAR 40-year reanalysis project. *Bull Am Meteorol Soc* 77:437–471.
- Lindesay JA, Andreae MO, Goldammer JG, Harris G, Annegarn HJ, Garstang M, Scholes RJ, van Wilgen BW. 1996. International geosphere–biosphere programme/international global atmospheric chemistry SAFARI-92 field experiment: background and overview. *J Geophys Res* 101:23521–30.
- Los SO, Justice CO, Tucker CJ. 1994. A global 1 degree by 1 degree NDVI data set for climate studies derived from the GIMMS continental NDVI data. *Int J Remote Sens* 15:3493–518.
- Malaisse F, Freson R, Goffinet G, Malaisse-Mousset M. 1975. Litter fall and litter breakdown in Miombo. In: Medina FBGaE, Eds. Tropical ecological systems: trends in terrestrial and aquatic research. Heidelberg: Springer-Verlag. pp 137–55.
- Mouillot F, Field CB. 2005. Fire history and the global carbon budget: a 1° × 1° fire history reconstruction for the 20th century. *Global Change Biol* 11:398–420.
- Nickeson J, Landis D, Privette JL, Morissette J. 2002. SAFARI 2000 Aerosol and fire products, satellite imagery. In: SAFARI 2000 CD-ROM Series, Vol. 2. National Aeronautics and Space Administration, Greenbelt, Maryland.
- Otter LB, Scholes RJ, Dowty P, Privette J, Caylor K, Ringrose S, Mukelabai M, Frost P, Hanan N, Totolo O, Veenendaal EM. 2002. The Southern African regional science initiative (SAFARI 2000): wet season campaigns. *South Afr J Sci* 98:131–137.
- Pender J, Jenner C, Wint W, Gilbert M. 2001. Programme against animal trypanosomiasis information system (PAATIS). Environmental Research Group Oxford Ltd on behalf of the Natural Resources Institute, Chatham.
- Potter CS, Randerson JT, Field CB, Matson PA, Vitousek PM, Mooney HA, Klooster SA. 1993. Terrestrial ecosystem production: a process model based on global satellite and surface data. *Global Biogeochem Cycles* 7:811–841.
- Prince SD, Goward S. 1995. Global primary production : a remote sensing approach. *J Biogeogr* 22:815–35.
- Ruimy A, Dedieu G, Saugier B. 1996. TURC: a diagnostic model of continental gross primary production and net productivity. *Global Biogeochem Cycles* 10:269–85.
- Scanlon TM, Albertson JD. 2004. Canopy scale measurements of CO<sub>2</sub> and water vapor exchange along a precipitation gradient in southern Africa. *Global Change Biol* 10:329–41.
- Scholes RJ. 1998. The South African 1:250 000 maps of areas of homogeneous grazing potential. Technical report CSIR.
- Scholes M, Andreae MO. 2000. Biogenic and pyrogenic emissions from Africa and their impact on the global atmosphere. *AMBIO* 29:23–29.
- Scholes RJ, Dowty PR, Caylor K, Parsons DAB, Frost PGH, Shugart HH. 2002. Trends in savanna structure and composition along an aridity gradient in the Kalahari. *J Veg Sci* 13:419–28.
- Scholes RJ, Frost PGH, Tian Y. 2004. Canopy structure in savannas along a moisture gradient on Kalahari sands. *Global Change Biol* 10:292–302.
- Scholes RJ, Kendall J, Justice CO. 1996. The quantity of biomass burned in southern Africa. *J Geophys Res* 101:23667–76.
- Scholes RJ, Walker BH, Eds. 1993. An African savanna: synthesis of the Nyilsvey study. New York: Cambridge University Press.
- Shea RW, Shea BW, Kauffman JB, Ward DE, Haskins CI, Scholes MC. 1996. Fuel biomass and combustion factors associated with fires in savanna ecosystems of South Africa and Zambia. *J Geophys Res* 101:23551–68.
- Simioni G, Le Roux X, Gignoux J, Sinoquet H. 2000. Treegrass: a 3D, process-based model for simulating plant interactions in tree-grass ecosystems. *Ecol Model* 131:47–63.

- Simpson J, Adler RF, North GR. 1988. A proposed tropical rainfall measuring mission (TRMM) satellite. *Bull Am Meteorol Soc* 69:278–95.
- Swap R. 2002. The southern African regional science initiative (SAFARI 2000): overview of the dry season field campaign. *South Afr J Sci* 98:125–30.
- Thomas DSG, Shaw PA. 1993. The evolution and characteristics of the kalahari, southern Africa. *J Arid Environ* 25:97–108.
- Thornthwaite CW. 1948. An approach toward a rational classification of climate. *Geogr Rev* 38:55–94.
- Trollope WSW, Trollope LA, Potgieter ALF, Zambatis N. 1996. SAFARI-92 characterization of biomass and fire behavior in the small experimental burns in the Kruger National Park. *J Geophys Res* 101:23531–9.
- UEA/CRU. 1990. An empirically derived adjustment factor for annual Thornthwaite PET estimates supplied under Phase II.
- van der Werf GR, Randerson JT, Collatz GJ, Giglio L. 2003. Carbon emissions from fires in tropical and subtropical ecosystems. *Global Change Biol* 9:547–62.
- van Wilgen BW, Scholes RJ. 1997. The vegetation and fire regimes of southern hemisphere Africa. In: Wilgen BW, Van, Andreae MO, Goldammer JG, Lindsay JA, Eds. *Fire in the southern African savannas: ecological and atmospheric perspectives*. Johannesburg: Witwatersrand University press. pp 27–46.
- Warnant P, Francois L, Strivay D, Gerard JC. 1994. CARAIB—a global model of terrestrial biological productivity. *Global Biogeochem Cycles* 8:255–70.
- Woodward FI, Lomas MR. 2004. Simulating vegetation processes along the Kalahari transect. *Global Change Biol* 10:383–92.
- Woodward FI, Smith TM, Emanuel WR. 1995. A global land primary productivity and phytogeography model. *Global Biogeochem Cycles* 9:471–90.